Current Research in Structural Biology 7 (2024) 100145

Contents lists available at ScienceDirect

Current Research in Structural Biology

journal homepage: www.journals.elsevier.com/current-research-in-structural-biology

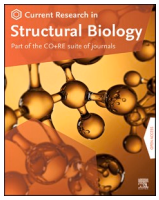

Research Article

Alternate conformations found in protein structures implies biological functions: A case study using cyclophilin A

Chandrasekaran Palaniappan [a,b,*], Santhosh Rajendran [a,b], Kanagaraj Sekar [a]

[a] Molecular Biophysics Unit, Indian Institute of Science, Bangalore, 560012, India
[b] Department of Computational and Data Sciences, Indian Institute of Science, Bangalore, 560012, India

ARTICLE INFO

Handling Editor: Prof G Oliva

Keywords:
Cyclophilin A (CypA)
Alternate conformations
Major and minor conformations
Molecular dynamics simulations

ABSTRACT

Protein dynamics linked to numerous biomolecular functions, such as ligand binding, allosteric regulation, and catalysis, must be better understood at the atomic level. Reactive atoms of key residues drive a repertoire of biomolecular functions by flipping between alternate conformations or conformational substates, seldom found in protein structures. Probing such sparsely sampled alternate conformations would provide mechanistic insight into many biological functions. We are therefore interested in evaluating the instance of amino acids adopted alternate conformations, either in backbone or side-chain atoms or in both. Accordingly, over 70000 protein structures appear to contain alternate conformations only 'A' and 'B' for any atom, particularly the instance of amino acids that adopted alternate conformations are more for Arg, Cys, Met, and Ser than others. The resulting protein structure analysis depicts that amino acids with alternate conformations are mainly found in the helical and β-regions and are often seen in high-resolution X-ray crystal structures. Furthermore, a case study on human cyclophilin A (CypA) was performed to explain the pre-existing intrinsic dynamics of catalytically critical residues from the CypA and how such intrinsic dynamics perturbed upon Ser99Thr mutation using molecular dynamics simulations on the ns-μs timescale. Simulation results demonstrated that the Ser99Thr mutation had impaired the alternate conformations or the catalytically productive micro-environment of Phe113, mimicking the experimentally observed perturbation captured by X-ray crystallography. In brief, a deeper comprehension of alternate conformations adopted by the amino acids may shed light on the interplay between protein structure, dynamics, and function.

1. Introduction

Proteins are dynamic biological entities that perform various cellular functions, such as catalysis, ligand binding, and allosteric regulation. X-ray crystallography and NMR spectroscopy are two powerful biophysical techniques that seize biological processes at the atomistic level. The resulting three-dimensional atomic coordinates thus inherently reveal critical aspects of biomolecular functions that typically occur within cells (Mittermaier and Kay, 2006; Boehr et al., 2006; Fraser et al., 2011). X-ray crystallography often provides macromolecular structures in a single static model. However, proteins can experience miscellaneous conformational dynamics in the crystalline medium, some of which are represented in the protein structures as alternate conformations. In general, electron density maps define the position of atomic coordinates of protein structures as determined by X-ray crystallography. Seldom, it covers a more extensive region for the atoms than its unique position. It meant the given electron density map contained more than one conformational state for the atoms, thus resulting in "alternate conformations" in the PDB file. The alternate conformations can be adopted by amino acids, either in the backbone or side chain atoms or in both. The PDB file defines the alternate conformations for any atoms assigned as 'A', 'B', etc. For example, the catalytic residue Phe113 from CypA (PDB ID: 3K0N) has an 'A' conformation with 0.63 occupancy while a 'B' conformation has 0.37 occupancy, based on the electron density map. However, any suitable conformational state between 'A' and 'B' conformations is also feasible; nevertheless, the residue coordinates are restricted between the two conformational states. (Miao and Cao, 2016; Santhosh et al., 2019; Keedy et al., 2015; van den Bedem et al., 2013; van den Bedem et al., 2013). Further, the role of alternate conformations has been studied in numerous cases (Fraser et al., 2009; Eisenmesser et al., 2005; Kawasaki et al., 2002; Colletier et al., 2006b), and even subtle conformational changes are sufficient to drive biomolecular

* Corresponding author. Molecular Biophysics Unit, Indian Institute of Science, Bangalore, 560012, India.
E-mail address: pcsdsci@gmail.com (C. Palaniappan).

https://doi.org/10.1016/j.crstbi.2024.100145
Received 23 September 2023; Received in revised form 16 March 2024; Accepted 15 April 2024
Available online 18 April 2024

functions (Koshland, 1998).

Determining the wide range of motions experienced by proteins in a crystal environment is a key challenge in X-ray crystallography. Because the uncertainty over whether the weak electron density signifies alternate conformations, noise, or model error, which eventually impedes amino acid structural heterogeneities (Levin et al., 2007; Lang et al., 2014; Terwilliger et al., 2007). Several computational approaches, such as Ringer (Lang et al., 2010), qFIT (van den Bedem et al., 2009), PHENIX (Adams et al., 2010), and FLEXR (Stachowski and Fischer, 2023), have been developed to solve this, as they can detect, refine and model the multiple conformations. Rather than focusing on a single conformation, these computational tools provide a promising opportunity to drive us toward numerous conformations for a greater understanding of the interplay between protein dynamics and function.

Given the significance of alternate conformations, this work presents in-depth analyses of protein structures with alternate conformations, highlighting the instance of amino acids with alternate conformations and their intended locations (α-helices, β-sheets, etc.). A better understanding of the discrete structural heterogeneities adopted by amino acids might bring new insights into protein dynamics linked with its function. Therefore, using all-atom molecular dynamics (MD) simulations on the ns-μs timescale, a case study on human cyclophilin A (CypA) was performed to replicate the functionally important alternate conformations captured by X-ray crystallography. CypA is a prolyl isomerase that catalyzes the *cis*/trans isomerization of a peptide bond of proline in substrates (Eisenmesser et al., 2005). Enzymatic activity of CypA is embedded in the X-ray crystal structure (PDB code: 3K0N), represented as alternate conformations, 'A' and 'B', for catalytically critical amino acids, including Arg55 and Phe113 (Fraser et al., 2009). However, the Ser99Thr mutation in CypA resulted in a 300-fold reduction in its catalytic activity due to inherent dynamics perturbations. Consequently, the mutant structure did not reflect alternate conformations for Arg55 and Phe113 (PDB code: 3K0O) as linked with the catalytic activity of CypA. The present study, therefore, attempts to reproduce the experimentally observed alternate conformations of the catalytically coupled residues from the CypA and explain the rationale for the observed disturbances of the catalytic residues in the Ser99Thr mutant using MD simulations on a μs-ns time scale.

2. Methods

2.1. Data collection

In the RCSB Protein Data Bank (PDB) (Burley et al., 2021), a total of 194,259 known three-dimensional structures of biological macromolecules have been reported as of August 11, 2022. Of these, only 80,046 entities show alternate conformations for certain residues, either in backbone or side-chain atoms or in both. The alternate conformations of any atom are identified by looking at the residue column of the PDB file. For example, the Cα atom of Phe113 from CypA (PDB ID: 3K0N) adopted 'A' and 'B' alternate conformations, represented as Cα APhe113 and Cα BPhe113. However, the same residue from the CypA upon Ser99Thr mutation (PDB ID: 3K0O) did not adopt alternate conformations, thus represented as Cα Phe113. Out of 80,046 protein structures, 79,045 entities were considered for further analysis as they showed only 'A' and 'B' alternate conformations for any atoms. Based on the experimental techniques, we further classified the number of protein structures that adopted alternate conformations, as shown in Table 1. In addition, to check if high-resolution structures often contain alternate conformations, we categorized the protein structures based on resolution (R). In addition, we also calculated the instance of amino acids with 'A' and 'B' alternate conformations for any atoms from a total of 78,132 protein structures determined by X-ray crystallography only and also identified their preferred positions (α-helix and β-sheet, etc.). DSSP program (Kabsch and Sander, 1983) was used to define the secondary structural elements of amino acids that adopted alternate conformations. The data set of this study includes protein structures in the apo form, complex with small molecules or with the components of macromolecules. All the structural analyses were performed using the PERL scripting programming language.

Table 1
Number of protein structures available in the Protein Data Bank (PDB) with alternate conformations.

As of August 11, 2022	
Number of macromolecular structures available in PDB	194259
Number of protein structures with alternate conformations	80046
Number of protein structures adopted only 'A' and 'B' alternate conformations	79045
Based on experimental techniques	**Number of structures**
X-ray crystallography	78132
Electron microscopy	713
Electron crystallography	18
Neutron diffraction	49
NMR spectroscopy	10
Hybrid	123
Protein structures with alternate conformations based on resolution (Å)	**Number of structures**
0 to 0.5 Å	2
0.5 to 1 Å	1113
1 to 1.5 Å	15592
1.5 to 2 Å	37838
2 to 2.5 Å	17803
2.5 to 3 Å	4915
>3 Å	869

2.2. Simulations setup

Human wild-type (wt) CypA (PDB code 3K0N: residues 2–164; R = 1.39 Å) and its Ser99Thr mutant (PDB code 3K0O; residues 2-165; R = 1.55 Å) (Fraser et al., 2009) X-ray crystallographic structures were used as initial atomic coordinates for molecular dynamics (MD) simulations. The major conformation of 3K0N (alternate conformation 'A', Occupancy 0.63) has been retained for wt-CypA. GROMACS v.2018.8 (Van Der Spoel et al., 2005) was used to perform an unbiased ns-μs timescale simulation with the GROMOS96 53a6 force field (Oostenbrink et al., 2004). The wt-CypA and its mutant were separately solvated in cubic boxes containing TIP3P water (Jorgensen et al., 1983) molecules and with 10 Å spacing between the protein and the edge of the box. To neutralize the charge of the system, counter ions, 3 Cl^- and 2 Cl^- were added to the wt-CypA and its mutant systems, respectively. Energy minimization using the steepest descent was used until the system converged at a maximum of 50,000 steps and $F_{max.}$ was <1,000 kJ mol-1 nm-1. Then, both systems were subjected to NVT and NPT equilibration of 2 ns each. The temperature was maintained at 300 K by a modified Berendsen thermostat, V-rescale (Bussi et al., 2007), while a Parrinello-Rahman barostat (Parrinello and Rahman, 1981) was used for pressure coupling at 1 bar. The particle mesh Ewald method (Darden et al., 1993) was used to calculate the electrostatic interactions with a grid spacing of 1.6. The Lincs algorithm (Hess et al., 1997) was used to constrain all bonds. The final production run is performed on an equilibrated system of wt-CypA and its mutant at a temperature of 300 K for 1,000 ns each using the leap-frog algorithm (Frenkel and Smit, 2001). Each conformation is saved at regular intervals of 10 ps (Chandrasekaran et al., 2019; Palaniappan et al., 2021).

2.3. Principle component analysis (PCA) and free energy landscape (FEL)

The mass-weighted covariance matrix of the protein was generated by subjecting the MD trajectories to PCA, describing the protein's dominant and collective modes (Amadei et al., 1993). This covariance

matrix is diagonalized to extract a set of eigenvectors and eigenvalues that reflect the molecule's concerted motion. Besides, the two-dimensional FEL is plotted by the joint probability distribution of two reaction coordinates. It can be evaluated by;

$$\Delta G(X) = -K_B T \ln P(X)$$

where *K*B denotes the Boltzmann constant, *T* signifies the temperature of the simulation, and *P*(*X*) is the probability distribution of conformations along the reaction coordinate *X*. This study considers the first and second Cartesian principal components (PCs) as reaction coordinates derived from PCA.

3. Results and discussion

3.1. Instance of amino acids adopted alternate conformations and their preferred secondary structural elements

Protein molecules are dynamic entities that undergo an ensemble of conformational changes to perform their functions. The high-resolution protein structures detemined by X-ray crystallography seldom contain conformational heterogeneity or alternate conformations for certain residues. They are typically designated in the protein structures based on their occupancy as 'A', 'B', etc (Miao and Cao, 2016; Santhosh et al., 2019). In recent years, much attention has been paid to studying alternate conformations of proteins, as they play a crucial role in various biomolecular functions (Fraser et al., 2009; Eisenmesser et al., 2005; Kawasaki et al., 2002; Colletier et al., 2006b). Therefore, probing experimentally derived alternate conformations adopted by the amino acids is critical because it may lead to a better understanding of the interplay between protein dynamics and its function. Thus, we considered only protein structures with alternate conformations for any atoms, specifically 'A' and 'B' conformations determined by X-ray crystallography. In this study, we only considered X-ray crystallographic structures because the other experimental approaches resolved only a limited number of protein structures with alternate conformations, thus excluded from this investigation (Table 1). Accordingly, 78,132 protein structures determined by X-ray crystallography displayed alternate conformations 'A' and 'B' for any atoms. High-resolution (1–2.5 Å) X-ray crystallographic protein structures often show alternate conformations, while low-resolution (>3 Å) structures rarely contain information about alternate conformations, as they are mainly hindered by lattice perturbations or greater protein flexibility (van den Bedem et al., 2009). It is important to note that the protein conformational diversity may also influence the adoption of alternate conformations for any atoms or residues. For example, the crystallographic structure of adenylate kinase 4 (PDB ID: 2AR7) has chains A and B, and each chain has shown conformational diversity concerning the globular RMSD (Monzon et al., 2016). Notably, Chain A from 2AR7 has shown alternate conformations for five residues and only one from Chain B. It appears that conformational diversity may be required for the amino acids to adopt alternate conformations, but not always. Because out of more than 14000 protein structures determined using NMR spectroscopy with more than one conformer or model, only 10 proteins adopted alternate conformations for any atoms.

We next calculated the instance of amino acids adopted alternate conformations 'A' and 'B' for any atoms and compared them with overall occurrences from 78,132 protein structures, as shown in Supplementary Table 1. Accordingly, amino acids Arg, Cys, Gln, Glu, Met, and Ser were found to adopt a higher percentage of alternate conformations when compared to their overall occurrence, while Ala is the least likely. The amino acids, as mentioned earlier, except Cys and Ser, share a similar structural resemblance with two or more side-chain dihedral angles, allowing them for a greater degree of conformational freedom, thus favoring the likelihood of adopting alternate conformations more frequently than others (Miao and Cao, 2016). Strikingly, the amino acids Cys and Met displayed the lowest overall count, though adopting alternate conformations at a higher percentage than the highest overall count of amino acids like Ala, Asp, Gly, Ile, Leu, Thr, and Val. Similar to Cys and Met, the amino acid Trp exhibited the lowest overall count, but the instance of Trp with alternate conformations was only 0.87 %. The difference in the instance of alternate conformations adopted by the amino acids might be related to their location on protein structure. The alternate conformations adopted by the aliphatic and aromatic residues (e.g., Ile, Leu, Val, Phe, Trp, and Tyr) showed the least percentage, while the charged amino acids (e.g., Arg, Glu, His, and Lys) had the highest percentage of alternate conformations. Indeed, hydrophobic residues constitute the protein's core and are less likely to frustrate and sustain packing efficiency; thus, alternate conformations may occur less frequently. Charged amino acids, on the other hand, are often found on the protein's surface and can undergo an ensemble of conformations, resulting in a higher percentage of alternate conformations, as reported elsewhere (Bhardwaj and Gerstein, 2009). Similar to the charged amino acids, hydrophilic amino acids Gln and Ser also had a higher percentage of alternate conformations, as they were likely located on the molecular surface of the protein. Notably, amino acids Ala, Gly, and Pro adopted alternate conformations with the lowest percentage, similar to aromatic amino acids (less than 1%). Furthermore, the alternate conformations that are adopted by the amino acids typically form the hydrogen bonds, have been broadly explored using acetylxylan esterase (AXE) (Ghosh et al., 2001). AXE catalyzes the deacetylation of xylan, nature's most abundant hemicellulose, via the catalytic triad Ser90-His187-Asp175. Aside from the catalytic triad, ten Ser and one Gln showed alternate conformations 'A' and 'B'. In both conformations, all residues form hydrogen bonds with either protein or solvent atoms. In more detail, the transition from 'A' to 'B' conformation of His187 requires the local structural rearrangement of other active site residues, particularly Tyr177. In the 'A' conformation, His187 forms a hydrogen bond with a water molecule, whereas Tyr177 has a van der Waals contact distance from the His187 side chain. The binding of sulfate ion to His187 *via* a hydrogen bond initiated the flip to the 'B' conformation, with Tyr177 shifting approximately 2 Å farther to accommodate His187. Consequently, the transition from the 'A' to 'B' conformation resulted in a net gain of two hydrogen bonds.

We also found instance of amino acids that adopted alternate conformations 'A' and 'B' in each secondary structural element and compared them to the overall count, as shown in Supplementary Table 2. The secondary structural elements of amino acids with alternate conformations have been defined using the DSSP program (Kabsch and Sander, 1983). According to the DSSP program, the β-ladder is defined as a set of one or more repeated bridges of identical type, while the β-sheet or bridge refers to a set of ladders connected by shared residues. The fundamental turn pattern is a single hydrogen bond that forms between residue types i and i + n (n = 3, 4, and 5). Bends are segments having more curvature. Chain curvature at the central residue i of five residues is measured as the angle formed by the backbone directions of the first three and last three residues. Supplementary Table 2 shows that the charged amino acid Arg preferred to adopt alternate conformations when situated in the β-ladder (4.72 %) compared to the other secondary structural elements. However, the overall instance of Arg with alternate conformations is about 4.06 % (Supplementary Table 1). Strikingly, the other three charged amino acids, Asp (1.48 %), Glu (2.66 %), and Lys (2.24 %) had the lowest percentage of alternate conformations while being in the β-ladder (Supplementary Table 2). However, the amino acids Asp (2.30 %), Glu (3.44), and Lys (3.00 %) preferred to sample the alternate conformations with higher percentages, while being found in the turn, α-helix, and β-sheet, respectively. Again, upon examining secondary structural elements, Gln strongly prefers adopting alternate conformations while in the π-helix (7.16 %), for Ser, its α-helix (7.34 %). In particular, Gln adopted alternate conformations with a two-fold increase when situated in the π-helix (7.16 %), compared to its overall percentage (3.12 %) (Supplementary Table 1). This analysis shows a

shred of information that the charged and polar amino acids Arg, Gln, Glu, and Ser appeared to adopt alternate conformations more instantly while positioned in the regular secondary structural elements. They are thought to offer key features to proteins *via* ion pairs, hydrogen bonding, and other non-specific electrostatic interactions. Electrostatic interactions contribute in various aspects, including protein structure, folding, binding, and other biological functions. The side chain atoms of amino acids, as mentioned earlier, are chemically active and can function as catalytic residues. They are primarily known to be involved in the bifunctional mechanisms: stabilizing transition states or other intermediates through electrostatic interactions and proton shuttling *via* protonation and deprotonation (Zhou and Pang, 2018). Thus, it might be the rationale for the higher instance of amino acids (Arg, Gln, Glu, and Ser) that adopted alternate conformations, which are likely required to perform the desired biomolecular functions by switching between distinct conformational substates. Furthermore, electrostatic interactions in CypA's catalytic activity have been widely explored (Camilloni et al., 2014; Li and Cui, 2003; Hamelberg and McCammon, 2009). According to Fraser et al. (2009), the electrostatic interactions of Arg55 most likely coupled with CypA's catalytic function by flipping between distinct conformations.

Furthermore, the hydrophobic amino acids Ile, Leu, and Val were found to adopt alternate conformations with the lowest percentage, while Met showed the highest percentage among the amino acids (Supplementary Table 1). However, Leu and Met preferred β-sheet, while Ile and Val favored turn and 3_{10}-helix regions, respectively (Supplementary Table 2), for sampling the alternate conformations with higher percentages. Among the 20 amino acids, Val is the highest abundance of amino acid that found in this large-scale data set (Supplementary Table 1) and known to be the most favorable structure-forming amino acid in proteins (total helical and β-regions) (Chou and Fasman, 1973). This observation may be argued if this branching, fork-like hydrophobic Leu performs a functional role. Strikingly, the functional role of Leu in numerous proteins have been reported such as myoglobin, hemoglobin, ferricytochrome C, insulin etc (Chou and Fasman, 1973). Amino acids with alternate conformations in the β-sheet may be located at the edge or termini. This is probably because the edges of the β-sheet are thought to be more accessible, as in the case of CypA (Fraser et al., 2009), which is thought to facilitate interactions with the substrate and the subsequent catalytic activity (Bartlett et al., 2002). The alternate conformations adopted by the hydrophobic amino acids may arise from the active site dynamics extended into the core via long-range concerted motion, as likely seen in CypA (van den Bedem et al., 2013; Fraser et al., 2009). Consequently, six Ile, three Leu, two Met, and five Val adopted alternate conformations 'A' and 'B', as represented in the X-ray crystallographic structure of CypA (PDB ID: 3K0N). Again, it has been reported that hydrophobic amino acids Ile, Leu, Met, and Val are more likely to be located at the interface of the homomers (Yan et al., 2008). Due to this structural propensity, the aforementioned amino acids can undergo an ensemble of conformational changes required for dimerization, which explains their possible adaption of alternate conformations. Furthermore, the aromatic amino acids Phe (0.79 %), Trp (0.87), and Tyr (0.88 %) adopted alternate conformations with the lowest overall percentage (Supplementary Table 1), though they prefer to sample the alternate conformations when positioned in turn (0.98 %), bend (1.10 %), and 3_{10}-helix (1.13 %) regions, respectively (Supplementary Table 2). Given their hydrophobicity, aromatic amino acids with alternate conformations occur less frequently, rendering them more buried and less prone to change conformations. Indeed, the role of alternate conformations adopted by the aromatic amino acid Phe has been studied broadly using acetylcholinesterase (AchE), which is likely involved in the hydrolysis of acetylcholine (Colletier et al., 2006a). It is reported that Phe330 from AchE is critical for both substrate entry into the active site and product release by flipping its aromatic ring. This quantitative analysis demonstrates that the difference in the instance of amino acids that adopted alternate conformations are closely related to the amino acid type, conformational freedom, and accessibility.

3.2. Case study on human cyclophilin A (CypA)

The role of side chain alternate conformations of the key catalytic residues of human cyclophilin A (CypA) and its Ser99Thr mutant has been studied extensively (Fraser et al., 2009). Substitution of Ser99 into Thr showed a 300-fold decrease in catalytic activity due to perturbations in alternate conformations of residues involved in catalysis. Therefore, a case study on CypA was performed to reproduce the catalytically coupled alternate conformations of Phe113 and explain what causes the perturbation in the intrinsic dynamics of Phe113 in the Ser99Thr mutant using molecular dynamics simulations ns-μs timescale. CypA is involved in *cis* and *trans* isomerization of peptide bonds in substrates. The active site is on one side of the molecule and consists of a cluster of hydrophobic residues, including the evolutionarily conserved Phe113. This hydrophobic pocket allows the preceding residue of the target proline to bind deeply into the catalytic cleft. However, the side chain guanidinium moiety of Arg55 promotes the isomerization process by forming hydrogen bonds with the substrate's prolyl nitrogen and weakening the peptide bond characteristic (Howard et al., 2003; Eisenmesser et al., 2002; Hamelberg and McCammon, 2009; Li and Cui, 2003). The catalytic mechanism of CypA has been regarded as a model for experimental and computational studies investigating the interplay between protein dynamics and its function (Fraser et al., 2009; Eisenmesser et al., 2005; Agarwal et al., 2004; Agarwal, 2004). Indeed, the intrinsic dynamics essential for the catalytic activity exist in the apo-form of the enzymes (Eisenmesser et al., 2005; Colletier et al., 2006b; Tobi and Bahar, 2005), which are reflected as alternate conformations in the X-ray crystal structure of CypA (PDB ID: 3K0N). In the Ser99Thr mutant, however, the catalytically coupled essential dynamics were perturbed; thus, functionally linked alternate conformations were not reported in the mutant structure (PDB code: 3K0O). A detailed understanding of these functionally relevant alternate conformations may provide mechanistic insights into CypA's catalytic activity.

3.2.1. Impairment in the catalytically active conformation of Phe113 in the mutant

The catalytically associated alternate conformations adopted by the residues proposed as "major" and "minor" states by taking account of a set of atomic coordinates defining the specific dihedral angles of χ1 (Phe 113, Ser/Thr99), χ2 (Met61), and χ3 (Arg55) (Fraser et al., 2009; Papaleo et al., 2014; Wapeesittipan et al., 2019). The major and catalytically active conformation of Phe113 corresponds to $\chi1 \approx 60^{\circ}$, while the minor, undefined, or inactive state corresponds to $\chi1 \approx -60^{\circ}$ (Fraser et al., 2009) are represented by sticks in Fig. 1A. The X-ray crystallographic structure of Ser99Thr has shown only the minor state for the Phe113 ($\chi1 \approx -60^{\circ}$), and the major conformation ($\chi1 \approx 60^{\circ}$) is not validated by the Ringer analysis (Lang et al., 2010). Therefore, this mutant structural model offers a chance to examine the extent to which MD simulations can reflect the conformational changes of Phe113. Interestingly, the MD simulations reproduce the experimentally derived major conformations of Phe113 in wt-CypA, except very few ensembles showing minor conformations, as shown in Fig. 1B. In contrast, the major and minor conformations of mutant Phe113 were equally populated, indicating that these two conformational substates are inverted. Notably, the major conformations of Phe113 from the mutant sampled during the simulation resemble the minor state of wt-CypA (Fig. 1A). Moreover, Phe113 is rapidly interconverted between the catalytically active and inactive forms in wt-CypA, consistent with the NMR data (Kern et al., 1995). However, the interconversion of the mutant Phe113 side chain appears to be slow, suggesting anomalies in the pre-existing intrinsic dynamics. Besides, the transition between the alternate conformations was estimated using parallel-tempering metadynamics (Papaleo et al., 2014), and the free energy difference for Ser99Thr was in good agreement with the experimental value of −2.5 kcal/mol (Otten

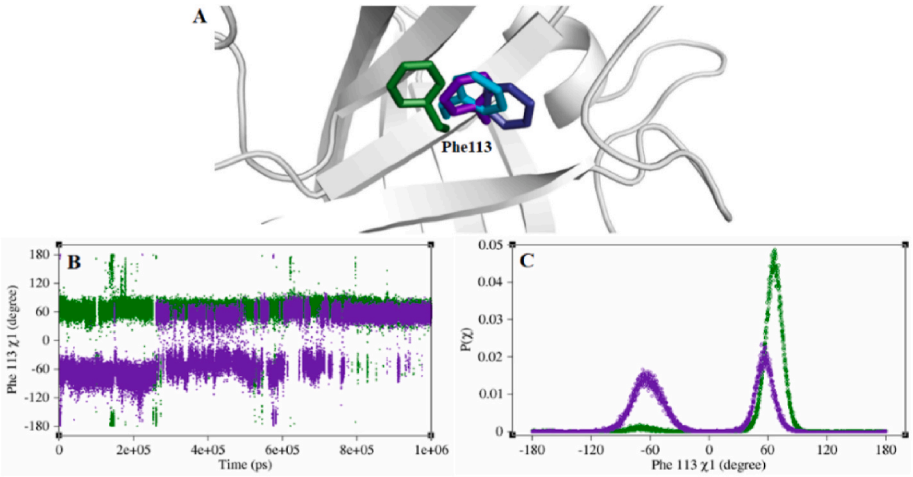

Fig. 1. Probing the catalytically coupled conformational sub-states of Phe113. The major (forest-green) and minor (cyan) conformations of the catalytically critical residue, Phe113, from wt-CypA and the major (purple-blue) and minor (deep-blue) conformations of Phe113 from mutant are shown by sticks. (B) Time evolution of the side-chain dihedral angle χ1 of Phe113 from wt-CypA (green) and its mutant (indigo) during ns-μs simulations and (C) their probability distributions.

et al., 2018). The rotamer profile of the other catalytically coupled residues is shown in Supplementary Fig. 1. It was found that the substituted amino acid Thr99 adopted two major conformational geometries for χ1 and distributed around at +60° and −60° in the mutant, as this pattern was not observed in the wt-CypA.

3.2.2. *Perturbation in the inherent dynamics of the mutant*

As discussed above, perturbation in the catalytically linked intrinsic dynamics of Phe113 from the mutant may be caused by the positional displacement of the Phe113 and its surrounding residues. Thus, Cα-RMSD is computed to probe the mutation-induced positional shift experienced by the residues by comparing it with wt-CypA during the 1000 ns simulations (Supplementary Fig. 2A). As expected, the substitution of Ser99 into Thr only with an additional methyl group showed a Cα-RMSD pattern similar to wt-CypA during the entire simulation period with a modest deviation at the globular level. To probe the region-specific structural changes influenced by Ser99Thr mutation on CypA in more detail, thus residue-wise Cα-RMSD is calculated (Supplementary Fig. 2B). Accordingly, in the Ser99Thr mutant, three regions have shown more Cα-RMSD deviations irrespective of mutational position, namely, (i) the coil regions (residues 42-45) connected at the C-terminal, the first and longest α-helix, (ii) the most extended coil region (residues 79-83) connecting β-strands 4 and 5, and (iii) the β-strand 7 (residues 111-116), indicating more conformational dynamics of those regions. It is now evident that the perturbation in the catalytically linked inherent dynamics of Phe113 from the mutant, as discussed earlier (Fig. 1B), is owing to the unrestrained conformational dynamics of β-strand 7. Besides, two other regions lost their inherent dynamics in the mutant by exhibiting lower Cα-RMSD values as compared to the wt-CypA, namely, (i) the C-terminal β-strand 1 and N-terminal β-strand 2 and its connecting region (residues 12-17) and (ii) the coil region between β-strand 5 and 6. Besides, the Cα-RMSF profile of wt-CypA and its mutant has followed a similar trend to the Cα-RMSD profile (Supplementary Fig. 2C). Altogether, the resulting RMSD and RMSF profiles imply an alteration in the catalytically productive environment of Phe113 from the mutant with increased frustration, as not conducive for the catalytic activity of CypA.

3.2.3. *Changes in the overall folding of the mutant*

As discussed earlier, the impairment in the intrinsic dynamics of Phe113 from the mutant may arise from changes in its structure compactness; thus, the radius of gyration (Rg) is calculated as an indicator of protein structure compactness (Supplementary Fig. 3A). Accordingly, the mutant exhibited a native-like compact structure around 500 ns, but structural relaxation likely started thereafter. The relaxation in the mutant structure after 500 ns attributed to the unrestrained conformational dynamics of two coil regions (residues 42-45 and 79-83) and the β-strand 7 (residues 111-116), as likely known from the residue-wise RMSD profile (Supplementary Fig. 2B). Strikingly, the catalytically linked Phe113 is positioned in the β-strand 7, which is found to be more frustrated. Therefore, we particularly replotted the Rg profile of Phe113 to explore in more detail how global structural changes affect the catalytically critical Phe113 (Supplementary Fig. 3B). It is worth noting that the ensemble of conformations produced during the 500 ns simulation period has shown higher Rg values for Phe113 despite adopting native-like structural compactness and corresponding to the catalytically inactive minor state. It appears that the mutant requires structural relaxation to adopt the major conformation of Phe113 corresponding to a lower Rg value. However, the major conformations of Phe113 from the mutant sampled after 500 ns resemble the minor conformations of wt-CypA. The extensive simulation result shows that the wt-CypA preserves the intrinsic dynamics of Phe113 required for catalysis, even in the apo state. Furthermore, it was reported that trivial (Zydowsky et al., 1992) or larger (Eisenmesser et al., 2005) displacement of Phe113 ultimately showed significant effects on CypA's catalytic activity. It is worth noting again that the Rg results obtained here indicate perturbation in both the local environment of Phe113 and at the globular level, in line with previous experimental results (Eisenmesser et al., 2005; Zydowsky et al., 1992).

3.2.4. *Uncertainty in the hydrophobic contacts brings perturbation in the catalytically critical conformational substates of Phe113*

The conformational transitions of the Phe113 side chain influence the *cis*-to-trans isomerization of proline in the substrate during catalysis and are likely driven by its major conformation (χ1 ~ 60°) (Fraser et al., 2009). However, such a functionally related conformational shift of Phe113 was found to be perturbed in the Ser99Thr mutant, as discussed earlier. It would be fascinating to probe the possible reason for the observed disturbance in the conformational equilibrium of Phe113; thus, we examined its dynamic network (Fig. 2A). Ensemble analysis revealed that the catalytically active major conformation of Phe113 from wt-CypA is likely stabilized by the hydrophobic contacts formed by Tyr48–Phe112 and Phe113–Leu122 (Fig. 2B) and also by its adjacent residue, Phe112. In the wt-CypA, only limited hydrophobic interactions were noticed between Phe112 and Phe129, demonstrating that these residues are more than 5 Å apart. This ensemble analysis suggests that these stable hydrophobic contacts may be necessary for preserving and determining the conformational substates of Phe113 required for the

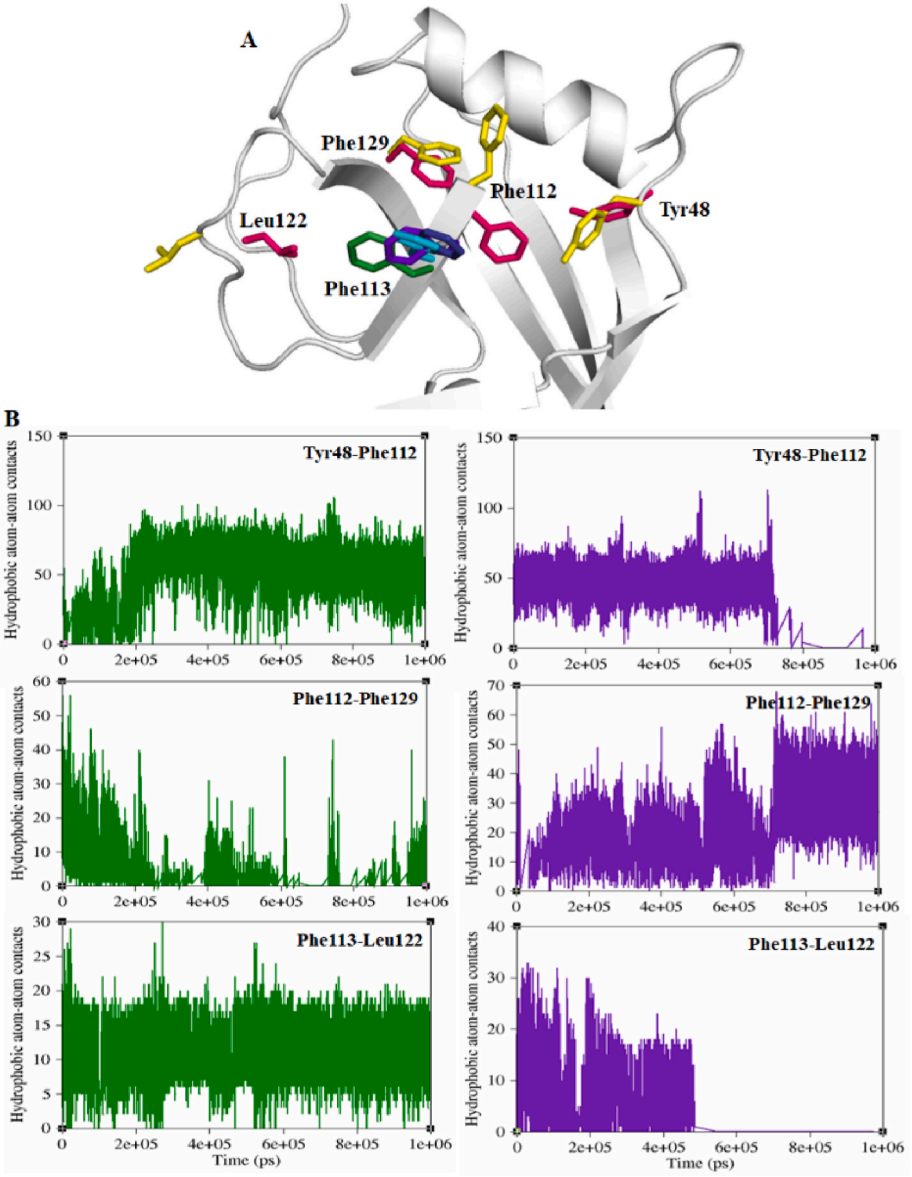

Fig. 2. Impairment in the hydrophobic pocket of the catalytic site. (A) The major (forest-green) and minor (cyan) conformations of the catalytically critical residue, Phe113, of wt-CypA, and the major (purple-blue) and minor (deep-blue) conformations of Phe113 of the mutant represented by sticks. The residues likely preserve the intrinsic dynamics of Phe113 are shown in the sticks for wt-CypA (deep-red) and mutant (yellow). (B) The number of hydrophobic atom-atom contacts formed between the residues from wt-CypA (green) and its mutant (indigo) during the 1000 ns simulations.

CypA catalytic activity. In the case of a mutant, the catalytically essential dynamic network is found to be perturbed (Fig. 2A), resulting in an atypical hydrophobic contact pattern (Fig. 2B). Like wt-CypA, stable hydrophobic contacts were also observed in the mutant and likely formed by Tyr48–Phe112 and Phe113–Leu122; however, these pair-wise contacts were absent after 700 and 500 ns, respectively. However, the side-chain dihedral angle of Phe113 equilibrates toward the catalytically inactive conformations until 700 ns (Fig. 1B). The loss of the hydrophobic contacts of Tyr48–Phe112 and Phe113–Leu122 after 700 and 500 ns, respectively, may be driven by the proximity between Phe112 and Phe129. It is worth mentioning that after 700 ns, the number of hydrophobic atom contacts that evolved between Phe112 and Phe129 was high, and the formation of aromatic-aromatic interaction was also possible. This unusual proximity between Phe112 and Phe129 allows the residue Phe113 to flip its $\chi1$ angle from -60° to $+60^\circ$, except for very few ensembles. However, the orientation of the major conformation ($\chi1 \sim +60^\circ$) resembles the catalytically inactive or minor conformation ($\chi1 \sim -60^\circ$) of wt-CypA. These observations suggest that the orientation of another and adjacent aromatic residue, Phe112, may be a critical factor in determining the conformational transition of Phe113. Our finding is also well corroborated with an earlier study, which reported the likely role of Phe112, and it was found to be involved in controlling the dynamic network of CypA by functioning as bottleneck residue (Doshi et al., 2016). The uncertainty in the hydrophobic catalytic site (Nagaraju et al., 2013), as seen here, could be the rationale for the perturbation in the conformational equilibrium of Phe113, as discussed earlier, which may be affected via perturbing Phe112.

3.2.5. Perturbation in Arg55 impaired the catalytic activity of Ser99Thr mutant

The evolutionarily well-conserved catalytic residue Arg55 plays a dual role in stabilizing the substrate transition state and catalysis (Howard et al., 2003; Eisenmesser et al., 2002; Hamelberg and McCammon, 2009; Li and Cui, 2003). It has also been reported that Arg55 substitution has a profound effect on the enzymatic activity of CypA. The catalytic activity (k_{cat}/k_m) of wt-CypA is estimated to be ~16

μM^{-1} S^{-1}, and for the Arg55Ala mutant, it was ~0.016 μM^{-1} S^{-1}, retaining only 0.1% of catalytic efficiency compared to the native CypA (Zydowsky et al., 1992). Similarly, CypA also showed a 300-fold decrease in its catalytic activity upon Ser99Thr mutation owing to the impairment in the catalytically productive microenvironment or alternate conformations of Phe113 (Fraser et al., 2009). In addition, Arg55 is known to play an important role in the catalytic mechanism of CypA via its guanidinium side chain; thus, monitoring its side chain dynamics would provide further insights into the reduced catalytic activity of CypA upon Ser99Thr mutation. Ensemble analysis exemplified that the side-chain guanidinium group of Arg55 from the mutant becomes proximity to Asn71, resulting in the formation of two unusual hydrogen bonds, Arg55:HE-Asn71:O and Arg55:HH21-Asn71:O (Fig. 3A), occurring only till 300 ns. These two atypical hydrogen bonds have most likely evolved owing to the positional shifts of both residues, Arg55 and Asn71. However, Arg55 from the mutant exhibited a side chain dihedral pattern for $\chi 3$ similar to the wt-CypA (Supplementary Fig. 1). As a result, the mutant shows a multimodal probability distribution for the distance of Arg55:HE-Asn71:O and Arg55:HH21-Asn71:O (Fig. 3B and C), suggesting changes in the intrinsic dynamics of the Arg55 side chain. The distance distribution with $\leq$3.5 Å further indicates the presence of non-native hydrogen bonds, as could not be seen in the wt-CypA. In the case of wt-CypA, a unimodal probability distribution was observed for the distance of Arg55:HE-Asn71:O and Arg55:HH21-Asn71:O and peaked at 12.5 Å as shown in Fig. 3B and C, respectively. Ensemble analysis demonstrated here that the Arg55 side chain from wt-CypA is anchored with evolutionarily conserved dynamics linked to its enzymatic activity. While the catalytically critical side-chain guanidinium group of Arg55 formed undesirable interactions with Asn71; therefore, the reactive atoms of Arg55 may not be available for enzymatic activity, as this may also be responsible for the 300-fold reduction in the catalytic activity of CypA upon Ser99Thr mutation. The extended ns-μs simulations demonstrated here the perturbations in the pre-existing intrinsic dynamics of the catalytically key residues, Arg55 and Phe113 in the mutant, which are known to be crucial for CypA's enzymatic activity.

3.2.6. *Impairment in the essential dynamics and folding pathways of the mutant*

The covariance matrices of the wt-CypA and its mutant, as shown in Supplementary Figs. 4A and B, respectively, demonstrate how atoms move around each other during the simulations. Positive correlation occurs when side chain atoms of two residues move in the same direction (red), while anti-correlation occurs when they move in the opposite direction (blue) or are uncorrelated (white). Strikingly, the side chain dynamics of residues from the mutant have been altered enormously; notably, the catalytically linked Phe113 and its adjacent residue 112 were negatively correlated, as circled in black (Supplementary Fig. 4B). In the wt-CypA, no such negatively and positively correlated dominant motions were noticed, except the commonly observed motions. Thus, both correlated and anti-correlated side chain motion of residues have evolved more in the mutant by comparing with wt-CypA. Thus, changes in the intrinsic side chain dynamics of residues in the mutant lead to perturbation in the residual network linked with catalytic activity, as discussed earlier (Fig. 2B). Further, the free energy landscape (FEL) has been generated by plotting the free energy (kJ/mol) versus the principal components 1 and 2, as depicted in Supplementary Fig. 5. It has been seen that wt-CypA has shown a well-defined folding pathway coupled with five low-energy basins. Meanwhile, the mutant displayed a broader exploration of folding intermediates and a single low-energy basin. Consequently, a significant difference in the free energy between the mutant (20.7 kJ/mol) and the wt-CypA (23.3 kJ/mol) has occurred. Again, it should be noted that the transition between one basin to another appeared rapidly in the wt-CypA, especially from basin 3 to basin 4 and basin 4 to basin 5. Inversely, it seems that the mutant appeared to explore more folding intermediates to attain the lowest free energy state. The more extensive exploration of folding intermediates, as seen in the mutant, primarily consists of catalytically inactive conformation of residue Phe113 ($\chi 1 \approx -60^{\circ}$).

Understanding the interplay between protein dynamics and function can be gained by careful examination of the alternate conformations adopted by the amino acids because even minor conformational changes can dictate protein function (Koshland, 1998). Therefore, precise representation of conformational polymorphisms adopted by the amino acids is critical for biomedical and biological research that relies on

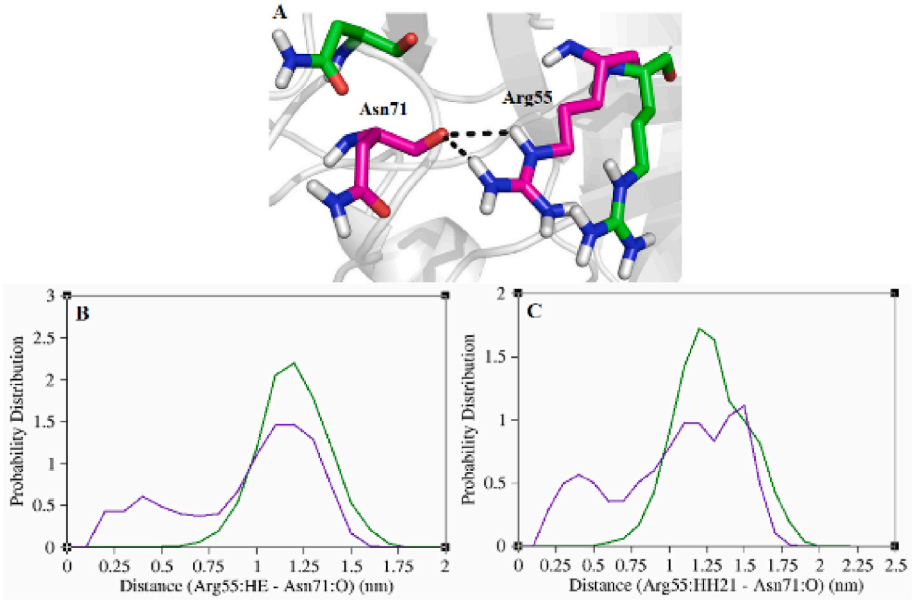

Fig. 3. Dynamic changes of catalytically essential Arg55 in the mutant. (A) The intrinsic dynamics of catalytically critical residue Arg55 from the mutant are perturbed by forming two non-native hydrogen bonds with Asn71 (Arg55:HE-Asn71:O and Arg55:HH21-Asn71:O), as this was not observed in the wt-CypA. The residues Arg55 and Asn71 from the wt-CypA (green) and its mutant (magenta) are represented by sticks. Dashed lines indicate hydrogen bonds. (B and C) Probability distribution of the distance between the side chain guanidinium moiety of Arg55 and the main chain carbonyl of Asn71 in wt-CypA (green) and its mutant (indigo).

structural data deposited in the PDB. In recent years, data collection at room temperature (298 K) has become relatively rare; instead, the cryogenic structures (100 K) dominate the PDB (Fraser et al., 2011). Although the cryogenic approach is believed to introduce a trivial bias in the backbone folding or hinder the conformational polymorphism of main- and side-chains or quenching the coupled dynamic network, as is likely the case with CypA (Fraser et al., 2011), DHFR (A Keedy et al., 2014), myoglobin (Frauenfelder et al., 1987; Frauenfelder et al., 1979), and RNase (Rasmussen et al., 1992; Tilton et al., 1992). The collection of X-ray crystallographic data at cryogenic temperatures was encouraged in the 1990s to avoid radiation damage during experiments (Haas and Rossmann, 1970; Hope, 1988). Therefore, crystal cooling and model building at the 1σ threshold can eliminate information regarding functionally relevant conformations instead of capturing the conformational distribution within the crystal. However, a recent study revealed a careful experimental design confirmed that radiation does not affect protein conformational dynamics at room temperature (Russi et al., 2017). Collecting room-temperature X-ray diffraction data can reveal the intrinsic dynamics required for ligand binding, catalysis, and allosteric regulation (Fraser et al., 2011). Thus, accurate representation of alternate conformations would help understand and manipulate the mechanisms of many macromolecular systems and may pave the way for new approaches in designing inhibitors for biomedically important systems.

4. Conclusions

The present study provides information regarding alternate conformations found in large-scale data of X-ray crystallographic protein structures. The resulting structural analysis revealed that high-resolution X-ray diffraction data often contain alternate conformations for either backbone or side chain atoms or in both. In particular, amino acids, such as Arg, Cys, Met, and Ser adopted alternate conformations more prevalently than others and are mainly located in the helical and β-regions. As evident from the case study, the catalytically productive microenvironment or alternate conformations of Phe113 were found to be perturbed, reported as explicit evidence for the decreased catalytic activity of CypA upon Ser99Thr mutation. In summary, a deeper understanding of alternate conformations adopted by amino acids will provide insights into the interplay between protein dynamics and function, and it could also oblige in designing inhibitors for biomedically important systems.

Funding

This work is supported by the Government of India's National Supercomputing Mission Platform for Genomics and Drug Discovery. CP and SR would like to thank the project titled "An Indian initiative on setting up a high-fidelity structural data archival/retrieval system for Life Science-(PDBi)". Reference code: (Meit/R&D/HPC/2(1)/2014).

CRediT authorship contribution statement

Chandrasekaran Palaniappan: conceived, designed, and performed the research, analyzed the results, and wrote & reviewed the manuscript. **Santhosh Rajendran:** Data curation. **Kanagaraj Sekar:** Supervision, project administration.

Declaration of competing interest

The authors declare no competing financial interest.

Data availability

Data will be made available on request.

Acknowledgments

The authors gratefully acknowledge the facilities provided by the Centre of Excellence in Structural Biology and Biocomputing, funded by the Department of Biotechnology (DBT), Government of India, and the Department of Computational and Data Sciences, Indian Institute of Science, Bangalore, India. The authors thank the anonymous reviewers for their insightful suggestions and constructive comments, which helped to improve the article's quality.

Appendix A. Supplementary data

Supplementary data to this article can be found online at https://doi.org/10.1016/j.crstbi.2024.100145.

References

Keedy, D.A., van den Bedem, H., Sivak, D.A., Petsko, G.A., Ringe, D., Wilson, M.A., Fraser, J.S., 2014. Crystal cryocooling distorts conformational heterogeneity in a model Michaelis complex of DHFR. Structure 22, 899–910.
Adams, P.D., Afonine, P.V., Bunkóczi, G., Chen, V.B., Davis, I.W., Echols, N., Headd, J.J., Hung, L.W., Kapral, G.J., Grosse-Kunstleve, R.W., et al., 2010. PHENIX: a comprehensive Python-based system for macromolecular structure solution. Acta Crystallogr. D Biol. Crystallogr. 66, 213–221.
Agarwal, P.K., 2004. Cis/trans isomerization in HIV-1 capsid protein catalyzed by cyclophilin A: insights from computational and theoretical studies. Proteins 56, 449–463.
Agarwal, P.K., Geist, A., Gorin, A., 2004. Protein dynamics and enzymatic catalysis: investigating the peptidyl-prolyl cis-trans isomerization activity of cyclophilin A. Biochemistry 43, 10605–10618.
Amadei, A., Linssen, A.B., Berendsen, H.J., 1993. Essential dynamics of proteins. Proteins 17, 412–425.
Bartlett, G.J., Porter, C.T., Borkakoti, N., Thornton, J.M., 2002. Analysis of catalytic residues in enzyme active sites. J. Mol. Biol. 324, 105–121.
Bhardwaj, N., Gerstein, M., 2009. Relating protein conformational changes to packing efficiency and disorder. Protein Sci. 18, 1230–1240.
Boehr, D.D., McElheny, D., Dyson, H.J., Wright, P.E., 2006. The dynamic energy landscape of dihydrofolate reductase catalysis. Science 313, 1638–1642.
Burley, S.K., Bhikadiya, C., Bi, C., Bittrich, S., Chen, L., Crichlow, G.V., Christie, C.H., Dalenberg, K., Di Costanzo, L., Duarte, J.M., et al., 2021. RCSB Protein Data Bank: powerful new tools for exploring 3D structures of biological macromolecules for basic and applied research and education in fundamental biology, biomedicine, biotechnology, bioengineering and energy sciences. Nucleic Acids Res. 49, 437–451.
Bussi, G., Donadio, D., Parrinello, M., 2007. Canonical sampling through velocity rescaling. J. Chem. Phys. 126, 014101.
Camilloni, C., Sahakyan, A.B., Holliday, M.J., Isern, N.G., Zhang, F., Eisenmesser, E.Z., Vendruscolo, M., 2014. Cyclophilin A catalyzes proline isomerization by an electrostatic handle mechanism. Proc. Natl. Acad. Sci. U. S. A. 111, 10203–10208.
Chandrasekaran, P., Santosh Kumar, C., Rangachari, K., Sekar, K., 2019. Disassociation of β1-α1-β2 from the α2-α3 domain of prion protein (PrP) is a prerequisite for the conformational conversion of PrP^{C} into PrP^{Sc}: driven by the free energy landscape. Int. J. Biol. Macromol. 136, 368–376.
Chou, P.Y., Fasman, G.D., 1973. Structural and functional role of leucine residues in proteins. J. Mol. Biol. 74, 263–281.
Colletier, J.P., Fournier, D., Greenblatt, H.M., Stojan, J., Sussman, J.L., Zaccai, G., Silman, T., Weik, M., 2006a. Structural insights into substrate traffic and inhibition in acetylcholinesterase. EMBO J. 25, 2746–2756.
Colletier, J.P., Sanson, B., Nachon, F., Gabellieri, E., Fattorusso, C., Campiani, G., Weik, M., 2006b. Conformational flexibility in the peripheral site of Torpedo californica acetylcholinesterase revealed by the complex structure with a bifunctional inhibitor. J. Am. Chem. Soc. 128, 4526–4527.
Darden, T., York, D., Pederesen, L., 1993. Particle mesh Ewald: an N.log(N) method for sums in large systems. J. Chem. Phys. 98, 10089–10092.
Doshi, U., Holliday, M.J., Eisenmesser, E.Z., Hamelberg, D., 2016. Dynamical network of residue-residue contacts reveals coupled allosteric effects in recognition, catalysis, and mutation. Proc. Natl. Acad. Sci. U. S. A. 113, 4735–4740.
Eisenmesser, E.Z., Bosco, D.A., Akke, M., Kern, D., 2002. Enzyme dynamics during catalysis. Science 295, 1520–1523.
Eisenmesser, E.Z., Millet, O., Labeikovsky, W., Korzhnev, D.M., Wolf-Watz, M., Bosco, D. A., Skalicky, J.J., Kay, L.E., Kern, D., 2005. Intrinsic dynamics of an enzyme underlies catalysis. Nature 438, 117–121.
Fraser, J.S., Clarkson, M.W., Degnan, S.C., Erion, R., Kern, D., Alber, T., 2009. Hidden alternative structures of proline isomerase essential for catalysis. Nature 462, 669–673.
Fraser, J.S., van den Bedem, H., Samelson, A.J., Lang, P.T., Holton, J.M., Echols, N., Alber, T., 2011. Accessing protein conformational ensembles using room-temperature X-ray crystallography. Proc Natl Acad Sci U S A 108, 16247–16252.
Frauenfelder, H., Petsko, G.A., Tsernoglou, D., 1979. Temperature-dependent X-ray diffraction as a probe of protein structural dynamics. Nature 280, 558–563.

Frauenfelder, H., Hartmann, H., Karplus, M., Kuntz, I.D.Jr., Kuriyan, J., Parak, F., Petsko, G.A., Ringe, D., Tilton, R.F.Jr., Connolly, M.L., et al., 1987. Thermal expansion of a protein. Biochemistry 26, 254–261.
Frenkel, D., Smit, B., 2001. Understanding Molecular Simulation: from Algorithms to Applications, vol. 1. Elsevier.
Ghosh, D., Sawicki, M., Lala, P., Erman, M., Pangborn, W., Eyzaguirre, J., Gutierrez, R., Jornvall, H., Thiel, D.J., 2001. Multiple conformations of catalytic serine and histidine in acetylxylan esterase at 0.90 A. J. Biol. Chem. 276, 11159–11166.
Haas, D.J., Rossmann, M.G., 1970. Crystallographic studies on lactate dehydrogenase at -75°C. Acta Cryst B26, 998–1004.
Hamelberg, D., McCammon, J.A., 2009. Mechanistic insight into the role of transition-state stabilization in cyclophilin A. J. Am. Chem. Soc. 131, 147–152.
Hess, B., Bekker, H., Berendsen, H.J.C., Fraaije, J.G.E.M., 1997. LINCS: a linear constraint solver for molecular simulations. J. Comput. Chem. 18, 1463–1472.
Hope, H., 1988. Cryocrystallography of biological macromolecules: a generally applicable method. Acta Cryst B44, 22–26.
Howard, B.R., Vajdos, F.F., Li, S., Sundquist, W.I., Hill, C.P., 2003. Structural insights into the catalytic mechanism of cyclophilin A. Nat. Struct. Biol. 10, 475–481.
Jorgensen, W.L., Chandrasekhar, J., Madura, J.D., Impey, R.W., Klein, M.L., 1983. Comparison of Simple Potential functions for simulating Liquid water. J. Chem. Phys. 79, 926–935.
Kabsch, W., Sander, C., 1983. Dictionary of protein secondary structure: pattern recognition of hydrogen-bonded and geometrical features. Biopolymers 22, 2577–2637.
Kawasaki, K., Kondo, H., Suzuki, M., Ohgiya, S., Tsuda, S., 2002. Alternate conformations observed in catalytic serine of Bacillus subtilis lipase determined at 1.3 A resolution. Acta Crystallogr. D Biol. Crystallogr. 58, 1168–1174.
Keedy, D.A., Fraser, J.S., van den Bedem, H., 2015. Exposing Hidden alternative backbone conformations in X-ray crystallography using qFit. PLoS Comput. Biol. 11, e1004507.
Kern, D., Kern, G., Scherer, G., Fischer, G., Drakenberg, T., 1995. Kinetic analysis of cyclophilin-catalyzed prolyl cis/trans isomerization by dynamic NMR spectroscopy. Biochemistry 34, 13594–13602.
Koshland, D., 1998. Conformational changes: how small is big enough? Nat. Med. 4, 1112–1114.
Lang, P.T., Ng, H.L., Fraser, J.S., Corn, J.E., Echols, N., Sales, M., Holton, J.M., Alber, T., 2010. Automated electron-density sampling reveals widespread conformational polymorphism in proteins. Protein Sci. 19, 1420–1431.
Lang, P.T., Holton, J.M., Fraser, J.S., Alber, T., 2014. Protein structural ensembles are revealed by redefining X-ray electron density noise. Proc Natl Acad Sci U S A 111, 237–242.
Levin, E.J., Kondrashov, D.A., Wesenberg, G.E., Phillips, G.N. Jr., 2007. Ensemble refinement of protein crystal structures: validation and application. Structure 15, 1040–1052.
Li, G., Cui, Q., 2003. What is so special about Arg 55 in the catalysis of cyclophilin A? insights from hybrid QM/MM simulations. J. Am. Chem. Soc. 125, 15028–15038.
Miao, Z., Cao, Y., 2016. Quantifying side-chain conformational variations in protein structure. Sci. Rep. 6, 37024.
Mittermaier, A., Kay, L.E., 2006. New tools provide new insights in NMR studies of protein dynamics. Science 312, 224–228.
Monzon, A.M., Rohr, C.O., Fornasari, M.S., Parisi, G., 2016. CoDNaS 2.0: a comprehensive database of protein conformational diversity in the native state. Database 2016, baw038.
Nagaraju, M., McGowan, L.C., Hamelberg, D., 2013. Cyclophilin A inhibition: targeting transition-state-bound enzyme conformations for structure-based drug design. J. Chem. Inf. Model. 53, 403–410.
Oostenbrink, C., Villa, A., Mark, A.E., van Gunsteren, W.F., 2004. A biomolecular force field based on the free enthalpy of hydration and solvation: the GROMOS force-field parameter sets 53A5 and 53A6. J. Comput. Chem. 25, 1656–1676.
Otten, R., Liu, L., Kenner, L.R., Clarkson, M.W., Mavor, D., Tawfik, D.S., Kern, D., Fraser, J.S., 2018. Rescue of conformational dynamics in enzyme catalysis by directed evolution. Nat. Commun. 9, 1314.
Palaniappan, C., Narayanan, R.C., Sekar, K., 2021. Mutation-Dependent Refolding of prion protein unveils amyloidogenic-related structural ramifications: insights from molecular dynamics simulations. ACS Chem. Neurosci. 12, 2810–2819.
Papaleo, E., Sutto, L., Gervasio, F.L., Lindorff-Larsen, K., 2014. Conformational changes and free energies in a proline isomerase. J. Chem. Theory. Comput. 10, 4169–4174.
Parrinello, M., Rahman, A., 1981. Polymorphic transitions in single crystals: a new molecular dynamics method. J. Appl. Phys. 52, 7182–7190.
Rasmussen, B.F., Stock, A.M., Ringe, D., Petsko, G.A., 1992. Crystalline ribonuclease A loses function below the dynamical transition at 220 K. Nature 357, 423–424.
Russi, S., González, A., Kenner, L.R., Keedy, D.A., Fraser, J.S., van den Bedem, H., 2017. Conformational variation of proteins at room temperature is not dominated by radiation damage. J. Synchrotron Radiat. 24, 73–82.
Santhosh, R., Chandrasekaran, P., Michael, D., Rangachari, K., Bankoti, N., Jeyakanthan, J., Sekar, K., 2019. ACMS: a database of alternate conformations found in the atoms of main and side chains of protein structures. J. Appl. Cryst. 52, 910–913.
Stachowski, T.R., Fischer, M., 2023. FLEXR: automated multi-conformer model building using electron-density map sampling. Acta Crystallogr D Struct. Biol. 79, 354–367.
Terwilliger, T.C., Grosse-Kunstleve, R.W., Afonine, P.V., Adams, P.D., Moriarty, N.W., Zwart, P., Read, R.J., Turk, D., Hung, L.W., 2007. Interpretation of ensembles created by multiple iterative rebuilding of macromolecular models. Acta Crystallogr. D Biol. Crystallogr. 63, 597–610.
Tilton, R.F.Jr., Dewan, J.C., Petsko, G.A., 1992. Effects of temperature on protein structure and dynamics: X-ray crystallographic studies of the protein ribonuclease-A at nine different temperatures from 98 to 320 K. Biochemistry 31, 2469–2481.
Tobi, D., Bahar, I., 2005. Structural changes involved in protein binding correlate with intrinsic motions of proteins in the unbound state. Proc Natl Acad Sci U S A 102, 8908–8913.
van den Bedem, H., Dhanik, A., Latombe, J.C., Deacon, A.M., 2009. Modeling discrete heterogeneity in X-ray diffraction data by fitting multi-conformers. Acta Crystallogr. D Biol. Crystallogr. 65, 1107–1117.
van den Bedem, H., Bhabha, G., Yang, K., Wright, P.E., Fraser, J.S., 2013. Automated identification of functional dynamic contact networks from X-ray crystallography. Nat. Methods 10, 896–902.
Van Der Spoel, D., Lindahl, E., Hess, B., Groenhof, G., Mark, A.E., Berendsen, H.J., 2005. GROMACS: fast, flexible, and free. J. Comput. Chem. 26, 1701–1718.
Wapeesittipan, P., Mey, A.S.J.S., Walkinshaw, M.D., Michel, J., 2019. Allosteric effects in cyclophilin mutants may be explained by changes in nano-microsecond time scale motions. Commun. Chem. 2, 41.
Yan, C., Wu, F., Jernigan, R.L., Dobbs, D., Honavar, V., 2008. Characterization of protein-protein interfaces. Protein J. 27, 59–70.
Zhou, H.X., Pang, X., 2018. Electrostatic interactions in protein structure, folding, binding, and condensation. Chem. Rev. 118, 1691–1741.
Zydowsky, L.D., Etzkorn, F.A., Chang, H.Y., Ferguson, S.B., Stolz, L.A., Ho, S.I., Walsh, C. T., 1992. Active site mutants of human cyclophilin A separate peptidyl-prolyl isomerase activity from cyclosporin A binding and calcineurin inhibition. Protein Sci. 1, 1092–1099.